OPEN ACCESS

University of BRISTOL

Peer reviewed version

Link to published version (if available):
10.1021/acs.macromol.9b00904

Link to publication record in Explore Bristol Research
PDF-document

## University of Bristol - Explore Bristol Research
### General rights

# Uniform, High Aspect Ratio, and Patchy 2D Platelets by Living Crystallization-Driven Self-Assembly of Crystallizable Poly(ferrocenyldimethylsilane)-based Homopolymers with Hydrophilic Charged Termini

Samuel Pearce,[†‡] Xiaoming He,[†§]  Ming-Siao Hsiao,[‖] Robert L. Harniman,[†] Liam R. MacFarlane,[†⊥] and Ian Manners[†⊥*]

† School of Chemistry, University of Bristol, Bristol BS8 1TS, United Kingdom

‡ Bristol Centre for Functional Nanomaterials, H.H. Wills Physics Laboratory, Tyndall Avenue, Bristol BS8 1TL

§ School of Chemistry and Chemical Engineering, Shaanxi Normal University, Xi'an 710119, China

‖ EI Dupont de Nemours and Co, DuPont R&D, Circleville, OH, USA

⊥ Department of Chemistry, University of Victoria, Victoria, BC V8W 3V6, Canada

**Abstract**

Two-dimensional (2D) seeded growth of poly(ferrocenyldimethylsilane) (PFS) homopolymers that possess hydrophilic charged termini in solution has been investigated using the living crystallization-driven self-assembly method. Charge-terminated homopolymers, $PFS_n[NMe_3]I$ were synthesized through a combination of living anionic polymerization and post-polymerization thiol-ene "click" chemistry.  Uniform and patchy high-aspect-ratio 2D structures were obtained by seeded growth in solution. We show that the aspect-ratio of the resultant 2D platelets could be controlled over a wide range (ca. 2 – 20) by changing either the solvent polarity of the medium in which seeded growth was conducted, the

substituents on the charged terminal group, or characteristics of the seed micelle. The counteranion associated with the charge-terminated PFS[NMe$_3$]$^+$ homopolymers was found to have a substantial effect on the resulting morphology and colloidal stability of the resulting 2D platelets and this may be a consequence of relatively high charge-density of the terminal quaternary ammonium cation.

**Introduction**

The self-assembly of block copolymers (BCPs) in solution is a well-established route to a wide array of micellar nano-particles (NPs).[1] These include morphologies such as spheres, cylindrical or worm-like micelles, and vesicles in addition to kinetically-trapped complex nanostructures such as multicompartment micelles.[2–7] Despite this, examples of two-dimensional (2D) structures by BCP self-assembly in solution are relatively rare as they tend to spontaneously undergo closure to form vesicles. Crystalline homopolymers are known to form 2D lamellae in solution due to the increased rigidity afforded upon crystallization[8] and thermal methods exist to control their size.[9] Without a solvophilic stabilising group or co-block, crystalline polymer lamellae aggregate resulting in precipitation from solution. Methods to produce colloidally-stable 2D polymer nanostructures in solution are of general interest.[10] For instance, homopolymer single crystals with various functional groups and BCPs with crystallizable core-forming blocks have been used to immobilise and template nanoparticles and to create chemical gradients for various applications.[11–14]

We have shown that the self-assembly of BCPs with a crystallizable poly(ferrocenyldimethylsilane) (PFS) core-forming block[15] in selective solvents for the complementary segment leads to PFS core-crystallization, favouring micelles of low-curvature at the core-corona interface, in a process called crystallization-driven self-assembly (CDSA).[15,16] 1D cylindrical structures are generally obtained at core:corona block ratios of 1:6 or above, whereas 2D platelets are formed from BCPs with a lower corona volume fraction.[17] It is also possible to favour the formation of 2D platelets through the blending of crystallizable homopolymer with a cylinder-forming BCP.[18] 2D platelet micelles can also be prepared from cylinder-forming BCPs with a core:corona block ratio 1:6 by increasing the relative volume fraction of common solvent in the solvent medium which acts as a plasticiser for the crystallizable core-forming block.[19]

A variety of other BCPs with a crystallizable core-forming block have been used to access colloidally-stable 2D platelets.[20–29] For example, poly(*l*-lactic acid)-*b*-poly(*N,N*-dimethylamino acrylate) (PLLA-*b*-PDMA) BCPs with various block ratios were observed to form 2D platelets in solution, in which BCPs featuring high corona:core block ratios favoured crystallization into 2D platelet micelles.[30] This exception to the general case that BCPs with low corona:core block ratios favour 2D structures was attributed to the greater solubility of the high corona:core block ratio BCPs in the selective

solvent which favours more extensive crystallization.[30] Poly(ethylene oxide) (PEO) BCPs also readily form 2D platelets and assemblies with concentric ring patterns by sequential addition of poly(ethylene oxide) PEO homopolymer and PEO-*b*-poly(styrene) (PEO-*b*-PS) to 2D platelets of the latter material.[31] Furthermore, functional 2D platelets formed of crystallizable π-conjugated polymers can be obtained *via* solution self-assembly protocols.[32,33]

In collaboration with Winnik and coworkers we have shown that 1D fiber-like BCP micelles with a crystalline core are active to the epitaxial growth of additional molecularly-dissolved BCP "unimer" in a process termed living CDSA, which is analogous to living covalent polymerisations of molecular organic monomers.[34,35] Uniform samples of 1D BCP micelles of controlled length are typically obtained by a "seeded growth" strategy, whereby initially generated polydisperse BCP micelles with crystalline cores are subjected to ultrasonication in solution causing fragmentation to generate small seed micelles which can subsequently be used as initiators. The length of the resulting fiber-like micelles can be controlled by the unimer-to-seed ratio and low length dispersities are obtained.[35] The living CDSA method has been most extensively studied for BCPs with a crystallizable PFS core-forming block,[36] but more recently this approach has been shown to be generally applicable to BCPs with a variety of crystallizable core-forming blocks including PLLA,[37] poly(ethylene),[38] poly(ε-caprol lactone),[39] poly(3-hexylthiophene),[40] poly(3-dodecylselenophene),[41] polyfluorenes,[42] polycarbonates,[43] and poly(p-phenylenevinylene).[44,45]

Analogous living CDSA approaches to produce uniform 2D platelets of controlled area have also been developed. Seeded growth of PFS-containing BCPs with a 1:1 block ratio produced uniform lenticular platelets with controllable area.[46] Living CDSA in 2D was demonstrated by the linear relationship between measured platelet areas and the unimer-to-seed mass ratio ($m_{unimer}/m_{seed}$). 1:1 blends by weight of cylinder-forming PFS-containing BCPs and PFS homopolymers form uniform patchy rectangular platelets of controllable area by living CDSA in 2D.[47] Uniform hollow structures were obtained by selective coronal cross-linking over defined regions of the platelet surface and subsequent dissolution of the platelet core. Seeded growth of BCP/homopolymer blends was recently extended to poly(ferrocenyldimethylgermane) (PFG)-containing polymers, through a heteroepitaxial growth mechanism using 1D PFS BCP seed micelles.[48] Living CDSA in 2D can also be extended to non-BCP systems, for instance square nanosheets of controllable dimensions can be formed from polyhedral oligomeric silsesquioxane-capped hyperbranched poly(ether amine) clusters through seeded growth in solution.[49]

We have recently reported a simplified protocol for the formation of 2D platelets with controlled dimensions via living CDSA.[50] These structures were obtained through seeded growth of phosphonium-terminated PFS homopolymers by 1D PFS-containing BCP 1D micelles. The platelet structures were colloidally stable in solution due to electrostatic repulsion between the charged surfaces which prevented stacking of crystalline lamellae. Kinetically-trapped hexagonal 2D morphologies could be obtained and sonication of these lamellae into 2D "seeds", followed by further addition of unimer yielded uniform hexagonal 2D nanocrystals via a "shape memory" effect.[50] All-organic 2D platelet structures can be

obtained by an analogous procedure using phosphonium-terminated poly(*l*-lactic acid) (PLLA) homopolymers, which demonstrated the generality of this approach.[51]

Our work on charge-terminated homopolymers to date has focussed upon expanding the scope of crystallizable homopolymers capped with a lipophilic methyl(diphenyl)phosphonium terminus.[50] Herein we report a study of the solution self-assembly of analogous crystallizable homopolymers with *hydrophilic* ammonium moieties as stabilising terminal groups for 2D homopolymer platelet micelles in polar solvents. This type of approach may ultimately offer a facile route to water soluble 2D assemblies for bio-related applications, as 2D BCP micelles with cationic ammonium surfaces have recently been shown to have promising anti-microbial properties[52] and act as oil-in-water emulsifiers.[53] With this in mind, herein we report the seeded growth of PFS homopolymers of low $DP_n$ with hydrophilic ammonium-termini in solution. Studies into the relationship between solvent polarity and the observed platelet morphology have been undertaken and new variables which affect the seeded growth of homopolymers in solution have been revealed.

**Results and Discussion**

**a) Synthesis and characterization of functionalised homopolymers**

The chemical structures of the polymers used in this study are shown in Figure 1. Phosphonium-terminated $PFS_{20}[PPh_2Me]I$ and green fluorescein dye-functionalised $PFS_{12}G$ homopolymers were synthesised according to previous literature using procedures briefly described as follows.[50] $PFS_{20}[PPh_2Me]I$ was prepared via living anionic polymerization by initiation of 1,1-dimethylsila[1]ferrocenophane in dry, degassed THF with *n*-butyl lithium solution in hexanes,[54] followed by quenching of the living anions with chlorodiphenylphosphine. Subsequent quaternization of the phosphine functional group was conducted by addition of a five-fold molar excess of methyl iodide to polymer solution in THF.[50] $PFS_{12}G$ was synthesized by addition of 1-aminoethanethiol to vinyl-terminated $PFS_{12}$ by thiol-ene click chemistry[55] and subsequently green fluorescein thioisocyanate was attached to the polymer chain terminus by stirring a THF solution of both the dye and amine-terminated polymer.[50] Charge-terminated $PFS_{12}[NMe_3]I$ homopolymer was synthesised via a 3-step procedure: Firstly, vinyl-terminated PFS homopolymer was prepared by living anionic polymerization, followed by quenching of the living anion with chlorodimethylvinylsilane. 2,2-(dimethylamino)ethanethiol was attached to the polymer terminus using well-established "thiol-ene click" chemistry.[55] Final quaternization of the dimethylamino functional group was achieved by methyl iodide at room temperature.[56] The number-average molecular mass $M_n$ of $PFS_{12}[NMe_3]I$ was found to be 2.92 kg/mol by matrix-assisted laser desorption time of flight (MALDI-TOF) mass spectrometry with a polydispersity $M_w/M_n = 1.08$, determined by gel permeation chromatography. The $M_n$ value determined was in agreement with that found by ^{1}H NMR end group integration. $PFS_{12}[NMe_2R]I$ (R = $C_6H_{13}$ or $C_{10}H_{21}$) homopolymers were synthesized similarly whereby 1-iodohexane or 1-iododecane was added to a THF solution of $PFS_{12}NMe_2$ and left under reflux for 12 h. Removal of residual neutral PFS homopolymer was achieved by precipitation into hexanes, a marginal solvent for PFS.

Following quaternization of the terminal tertiary amino group, a quantitative change in chemical shift from *ca.* 2.2 ppm to 3.2 ppm was observed by integration of the N*Me3* proton resonance in the $^1$H NMR spectra (Figure S1). No CH$_3$ resonance associated with the neutral tertiary amino group was observed in the $^1$H NMR spectrum of PFS$_{12}$[NMe$_3$]I (Figure S1). Quantitative end-capping, *ca.* 99% efficiency, of the homopolymers was determined using integration of the proton resonances, Cp*H* (4.2 ppm) in the polymer backbone and N*Me3* (3.2 ppm) terminus within the $^1$H NMR spectrum and MALDI-TOF mass spectrometry (Figures S1, S2 and S3). Addition of the tertiary amine and methyl group could be observed by mass shifts corresponding to the termini in the MALDI-TOF spectra of each reaction product (Figure S2d). The characteristics of the ammonium-terminated homopolymers are summarized in Table 1.
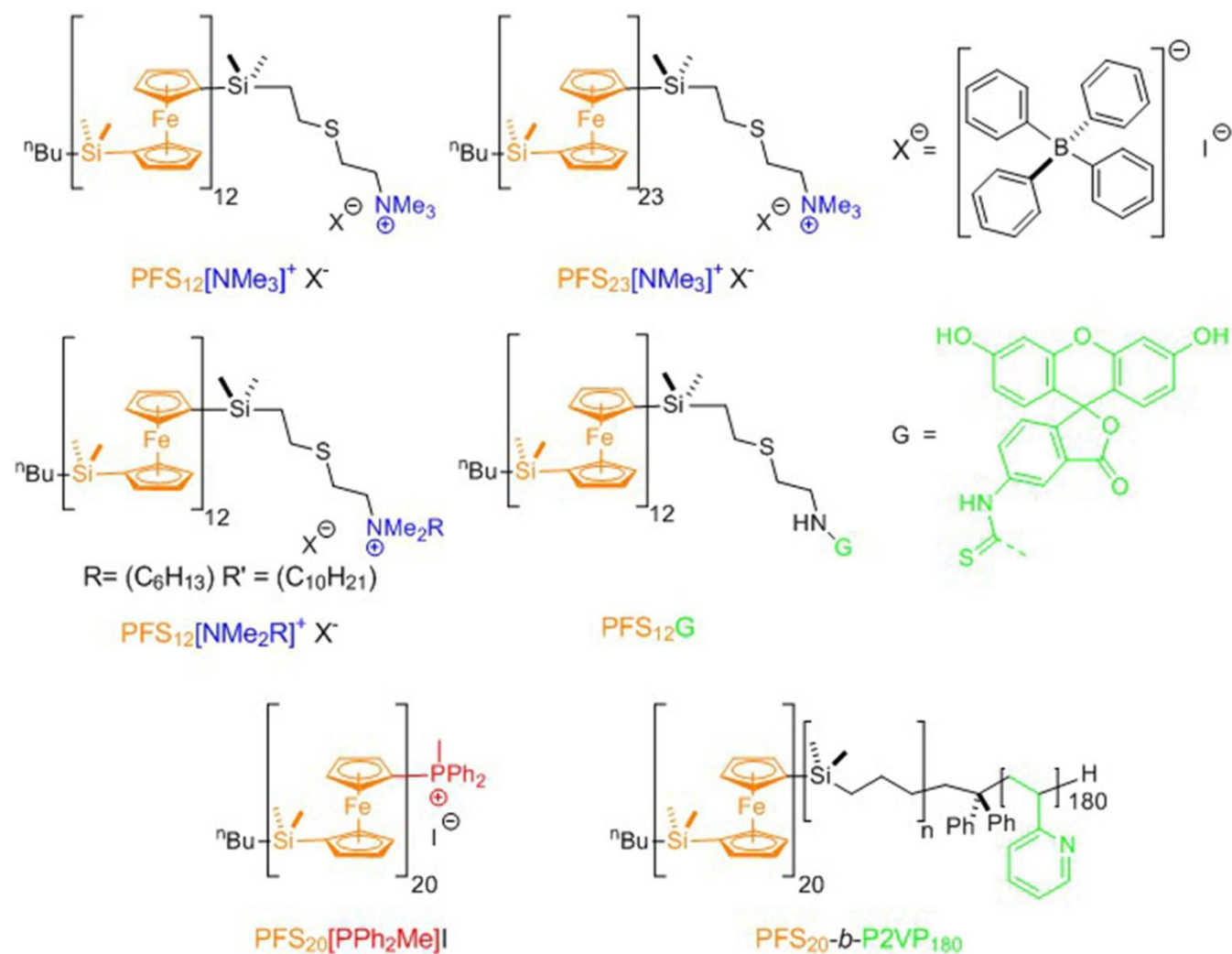


**Figure 1**. Chemical structures of the synthesized polymers used in this study.

**Table 1. Number-Average Molecular Weights ($M_n$) and Polydispersity Indices (PDI) of ammonium-terminated homopolymers used in this study**

| Sample | $M_n{}^a$ (kg/mol) | Đ[b] |
|---|---|---|
| PFS$_{12}$[NMe$_3$]I | 2.92 | 1.08 |
| PFS$_{12}$[NMe$_2$(C$_6$H$_{13}$)I | 2.69 | 1.05 |
| PFS$_{12}$[NMe$_2$(C$_{10}$H$_{21}$)]I | 2.72 | 1.05 |
| PFS$_{23}$[NMe$_3$]I | 5.81 | 1.04 |

[a] Determined by MALDI-TOF mass spectrometry [b] Determined by GPC analysis relative to polystyrene standards

## b) Formation of high-aspect-ratio platelet micelles by seeded growth

Self-assembly of PFS$_{12}$[NMe$_3$]I by rapid injection of polymer solution in THF over 0.1 s to isopropanol (iPrOH), in the absence of seed micelles resulted in only spherical aggregates being observed by bright-field TEM microscopy (Figure S4). This could be attributed to the large polarity difference between the hydrophilic ammonium-iodide ion pair and the hydrophobic PFS chain causing rapid precipitation of the PFS core-forming block into kinetically-trapped spherical micelles which presumably have an amorphous core. A similar effect has been observed for neutral BCPs with a crystallizable core-forming block. For example the self-assembly of PFS-b-poly(2-vinyl pyridine) (P2VP) BCPs by addition of the polymer solution in THF to methanol at room temperature resulted in the formation of spheres.[19,57,58] Addition of iPrOH (1 mL/h) to a 1 mg/mL solution of PFS$_{12}$[NMe$_3$]I in THF over 2 h resulted in the formation of 2D aggregated structures of ill-defined shape (Figure S5). There was no observable presence of spherical micelles in the latter case, which is attributed to the slow addition of the selective solvent providing sufficient time for crystallization of the PFS segment.

We then attempted seeded growth of PFS$_{12}$[NMe$_3$]I homopolymer from cylindrical PFS$_{20}$-b-P2VP$_{180}$ seed micelles in solution ($L_n$ = 260 nm, $L_w/L_n$ = 1.04, where $L_w$ is the weight-average length and $L_n$ is the number-average length). 1D PFS$_{20}$-b-P2VP$_{180}$ seed micelles were prepared by a 3-step process. Solid BCP was first dissolved in iPrOH/THF 4:1 v/v at 70 °C, followed by slow cooling to 25 °C over 12 h, to produce polydisperse 1D micelles. Sonication of these long, polydisperse PFS$_{20}$-b-P2VP$_{180}$ micelle fibers for 1 h at -78 °C produced fragments, which were used as seed initiators for the seeded growth of further PFS$_{20}$-b-P2VP$_{180}$ unimers to obtain uniform micelles ($L_n$ = 260 nm) to function as seeds for living CDSA in 2D (Figure S6).[34,35]

Seeded growth of $PFS_{12}[NMe_3]I$ in $i$PrOH from 1D $PFS_{20}$-$b$-$P2VP_{180}$ micelles was conducted by injection of a polymer solution in THF (5 mg/mL) over 0.1 s to dilute solutions of seed micelles in $i$PrOH (Figure 2a). Solutions were left for 24 h, prior to drop-casting of an aliquot for analysis by bright-field TEM microscopy. The seeded growth yielded relatively well-defined, high-aspect-ratio ribbon-like platelets, observed by bright-field TEM imaging and the area of the ribbon-like platelets was found to be linearly dependent on the unimer-to-seed mass ratio ($m_{unimer}/m_{seed}$) (Figure 2b-c). The contour areas for the platelets are summarised in Supplementary Table 2 and histograms of the contour area distributions are displayed in Figure S7. Area dispersities ($A_w/A_n$) of the platelets were observed to consistently remain below 1.1, typical with a living growth process. The $PFS_{20}$-$b$-$P2VP_{180}$ seed micelle in the center of the structures was easily observable through the electron contrast in bright-field TEM images due to the long P2VP coronal block (Figure 2c-e). The charged surface of the platelet micelle provided colloidal stability in the polar solvent medium presumably due to electrostatic repulsions however slow aggregation was detected over a period of weeks.
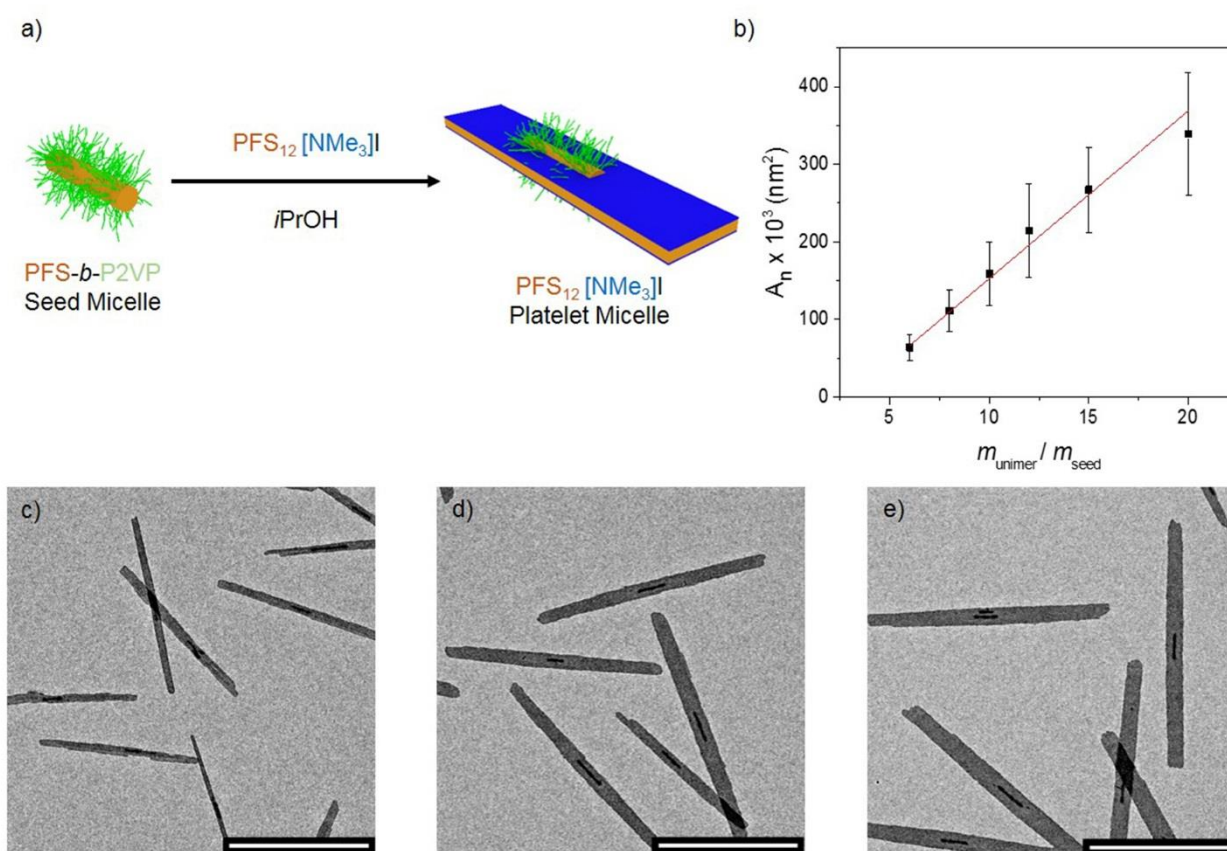


**Figure 2.** a) Cartoon schematic representation for the formation of 2D high-aspect-ratio platelets by seeded growth of $PFS_{12}[NMe_3]I$ from 1D $PFS_{20}$-$b$-$P2VP_{180}$ micelles ($L_n = 260$ nm, $L_w/L_n = 1.04$). b) Graph depicting the linear dependence of micelle area on the $m_{unimer}/m_{seed}$ ratio, indicative of a living-growth mechanism. Error bars are the standard deviation of measured areas. (c-e) Bright-field TEM images of platelet micelles prepared by the seeded growth of $PFS_{12}[NMe_3]I$ in

THF solution (5 mg mL$^{-1}$) from a solution of 1D seed micelles in $i$PrOH at 23 °C, at different unimer-to-seed mass ratios ($m_{unimer}/m_{seed}$) (c) 6 (d) 10 (e) 20. Scale bars = 2000 nm.

The homopolymer platelet height was found to be *ca.* 8.5 nm by atomic force microscopy (AFM) analysis in height mode. The central cylindrical seeds were observed to be substantially higher (14 nm), presumably due to the presence of the long corona-forming P2VP block (Figure 3 and Figure S8). Using the literature value of 6.9 Å for a Fe-Fe distance in the main chain of a fully-chain-extended crystalline PFS polymer,[59] the theoretical length of the PFS$_{12}$ core was calculated to be 8.3 nm. Considering the additional length contribution from the terminal group, a height of *ca.* 8.5 nm is consistent with the platelets possessing a fully-chain-extended polymer PFS chains without chain-folding in the crystalline core.
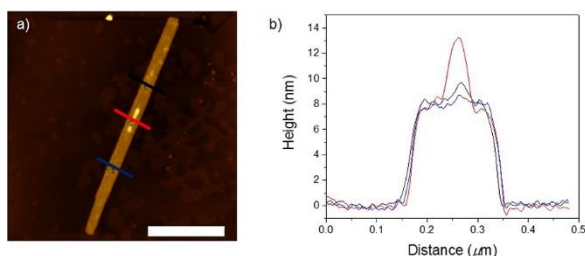


**Figure 3.** AFM topological image of a PFS$_{12}$[NMe$_3$]I micelle drop-cast onto mica from $i$PrOH and corresponding linear height profile. $m_{unimer}/m_{seed}$ = 10. Scale bar = 1000 nm.

Selected area electron diffraction (SAED) analysis of the high-aspect-ratio platelet micelles revealed three identical pairs of ED spots consistent with the literature[19] characterization of a single-crystal PFS micelle with a monoclinic unit cell and a lattice parameter $d$ spacing of 6.3 Å (Figure S9). The ED pattern was observed to be consistent for both the PFS$_{20}$-$b$-P2VP$_{180}$ 1D seed micelle and surrounding PFS$_{12}$[NMe$_3$]I platelet consistent with the growth of the latter via an epitaxial growth process.[19,60]

The aspect ratios ($L_n/W_n$) of the PFS$_{12}$[NMe$_3$]I platelets formed through seeded growth from 1D PFS$_{20}$-$b$-P2VP$_{180}$ micelles ($L_n$ = 260 nm, $L_w/L_n$ = 1.04) are high, ranging in values from 27 to 18 as $m_{unimer}/m_{seed}$ increases from 8 to 20. These values are far greater than those observed previously by the seeded growth of PFS$_{20}$[PPh$_2$Me]I from PFS-$b$-P2VP seed fibers in $i$PrOH, which were observed to vary from 14 to 3.[50] Seeded growth of a phosphonium-terminated PFS homopolymer of similar DP$_n$, PFS$_{11}$[PPh$_2$Me]I from PFS$_{20}$-$b$-P2VP$_{180}$ 1D seed micelles ($L_n$ = 260 nm, $L_w/L_n$ = 1.04) in $i$PrOH at $m_{unimer}/m_{seed}$ = 10, yielded platelets with $L_n/W_n$ = 7.1 (Figure S10). This is significantly lower than the analogous platelet aspect ratios formed from PFS$_{12}$[NMe$_3$]I by seeded growth, which indicates that the DP$_n$ of the PFS homopolymer is not responsible for the difference.

The difference in aspect ratio arising from the presence of different charged end-groups reflects the relative rates of longitudinal and lateral growth relative to the seed direction. The factors that affect these parameters are not clear at this

stage. The aspect ratio of the platelets decreased as the value of $m_{unimer}/m_{seed}$ increased ($L_n/W_n$ decreased from 27 to 18 as $m_{unimer}/m_{seed}$ increases from 8 to 20, Figure S7b), which has been previously noted[50] and presumably reflects the increased area at the platelet edge available for lateral growth as the living CDSA process initially proceeds in the longitudinal direction from the seed termini.

We also attempted to transfer a sample of the 2D assemblies into water. Specifically, a sample of high-aspect-ratio PFS$_{12}$[NMe$_3$]I platelet micelles in $i$PrOH ($A_n = 341 \times 10^3$ nm$^2$, $A_w/A_n = 1.05$, $L_n/W_n = 15.6$, 0.1 mg/mL) was dialysed into water. After 12 h, a precipitate could be observed in the dialysis tubing. Subsequent TEM analysis of the precipitate showed that the platelet micelles aggregated and fragmented upon transfer from organic to aqueous media (Figure S11). This indicates that a single charged terminal ammonium group is unable to colloidally stabilise the 2D platelet micelle in aqueous media presumably as the PFS core-forming block is very hydrophobic.

**c) Effect of *N*-alkyl substituents and solvent polarity upon 2D seeded growth of ammonium-terminated PFS homopolymers in solution**

In order to study how the self-assembly behavior of the ammonium-terminated homopolymers is influenced by the length of alkyl substituents attached to the quaternary amino group, 1-iodohexane and 1-iododecane were used as quaternization reagents. Seeded growth of PFS$_{12}$[NMe$_2$R]I (where R = C$_6$H$_{13}$ or C$_{10}$H$_{21}$) in $i$PrOH, from 1D PFS$_{20}$-$b$-P2VP$_{180}$ micelle fibers ($L_n = 260$ nm, $L_w/L_n = 1.04$), yielded high-aspect-ratio platelets (17.8 and 16.7 for R = C$_6$H$_{13}$ or C$_{10}$H$_{21}$) respectively) in solution irrespective of the terminal group (Figure S12). This result indicated that introducing long, hydrophobic aliphatic carbon chains onto the charged terminus has little effect upon the self-assembly behavior.

We also studied seeded growth of PFS$_{12}$[NMe$_2$R]I (where R = Me, C$_6$H$_{13}$ or C$_{10}$H$_{21}$) from 1D PFS$_{20}$-$b$-P2VP$_{180}$ micelles ($L_n = 260$ nm, $L_w/L_n = 1.04$) in MeOH (rather than $i$PrOH). This also yielded 2D platelet structures, observed by bright-field TEM imaging (Figure 4b-d). However, for PFS$_{12}$[NMe$_3$]I relatively irregular 2D platelet structures were obtained (Figure 4b) whereas seeded growth of PFS$_{12}$[NMe$_2$R]I (R= C$_6$H$_{13}$ or C$_{10}$H$_{21}$) in MeOH led to more regular platelet structures (Figure 4c, d).

Significantly, all of the 2D platelets formed by seeded growth in MeOH were noticeably lower in aspect ratio than those formed in $i$PrOH. To allow a quantitative comparison, platelets were formed by seeded growth with a $m_{unimer}/m_{seed}$ value of 10 in both MeOH and $i$PrOH. The 2D platelets formed by PFS$_{12}$[NMe$_2$(C$_6$H$_{13}$)]I were found to have an average aspect ratio of 4.7 in MeOH compared to 17.8 in $i$PrOH. For the case of PFS$_{12}$[NMe$_2$(C$_{10}$H$_{21}$)]I the average aspect ratios in the different solvents showed the same trend ($L_n/W_n$ values are 4.4 in MeOH vs 16.7 in $i$PrOH). The formation of platelets with ca. 4 times the aspect ratio in $i$PrOH compared to MeOH is presumably a consequence of the higher polarity of the latter solvent. However, how this would influence the rate of longitudinal versus lateral growth is unclear. Detailed studies

9

of the kinetics of living CDSA in 1D have only recently been performed and demonstrated that the quality of the solvent medium for the crystallizable segment greatly affects the epitaxial growth rate.[36] Analogous studies for 2D growth would be of substantial value.
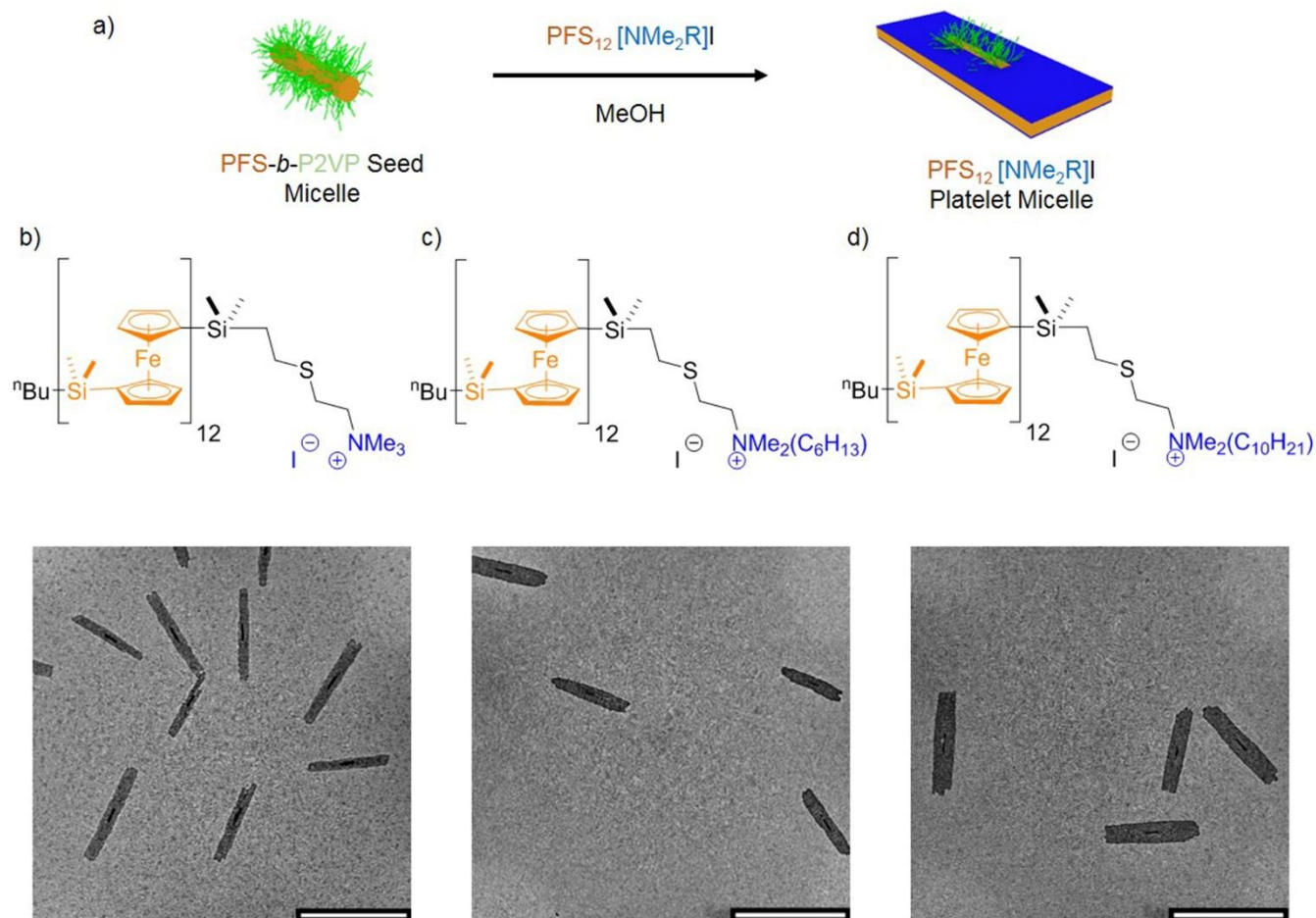


**Figure 4.** a) Cartoon schematic representation of the formation of 2D high-aspect-ratio platelets formed through seeded growth of PFS$_{12}$[NMe$_2$R]I (where R is CH$_3$, C$_6$H$_{13}$ or C$_{10}$H$_{22}$) from 1D PFS$_{20}$-$b$-P2VP$_{180}$ cylindrical seeds in MeOH. b-d) Bright-field TEM images of platelet structures formed through seeded growth of PFS$_{12}$[NMe$_3$]I, PFS$_{12}$[NMe$_2$(C$_6$H$_{13}$)]I and PFS$_{12}$[NMe$_2$(C$_{10}$H$_{21}$)]I homopolymers by PFS$_{20}$-$b$-P2VP$_{180}$ cylindrical micelles ($L_n$ = 260 nm, $L_w/L_n$ = 1.04) in MeOH. $m_{unimer}/m_{seed}$ = 10. Scale bars = 2000 nm.

The effect of solvent medium polarity upon the 2D platelet aspect ratio was further investigated by conducting seeded growth experiments of PFS$_{12}$[NMe$_2$(C$_{10}$H$_{22}$)]I from PFS$_{20}$-$b$-P2VP$_{180}$ seed micelles ($L_n$ = 260 nm, $L_w/L_n$ = 1.04) in a number of different solvents, of various polarity (Figure 5a). Seeded growth at $m_{unimer}/m_{seed}$ = 10 was performed in each experiment. The data indicates that there is a reasonable correlation between the 2D platelet aspect ratio ($L_n/W_n$) and solvent polarity as defined by Reichart, E$_T$(30) (30 refers to the negatively solvatochromic pyridiniophenolate dye used to derive the longest-wavelength UV-Vis absorption band, at a defined absolute temperature T (25 °C)) (Figure 5b).[61] A more detailed list of the platelet lateral dimensions in defined solvents is shown in Supplementary Table 1. Figure 5c and

10

Figure S13 show bright-field TEM images of the platelets obtained by seeded growth in the different solvents. It was possible to obtain uniform platelet micelles of identical composition with aspect ratios varying from 1.9 (obtained by seeded growth in DMF) to 22.4 (obtained by seeded growth in butan-2-ol) by variation of the solvent medium. We presume that the difference in platelet aspect ratio obtained by seeded growth in solvents of similar polarity such as MeCN and butan-2-ol are due to other contributing factors, such as the solubility of the charged terminus and PFS core-forming block in each medium.
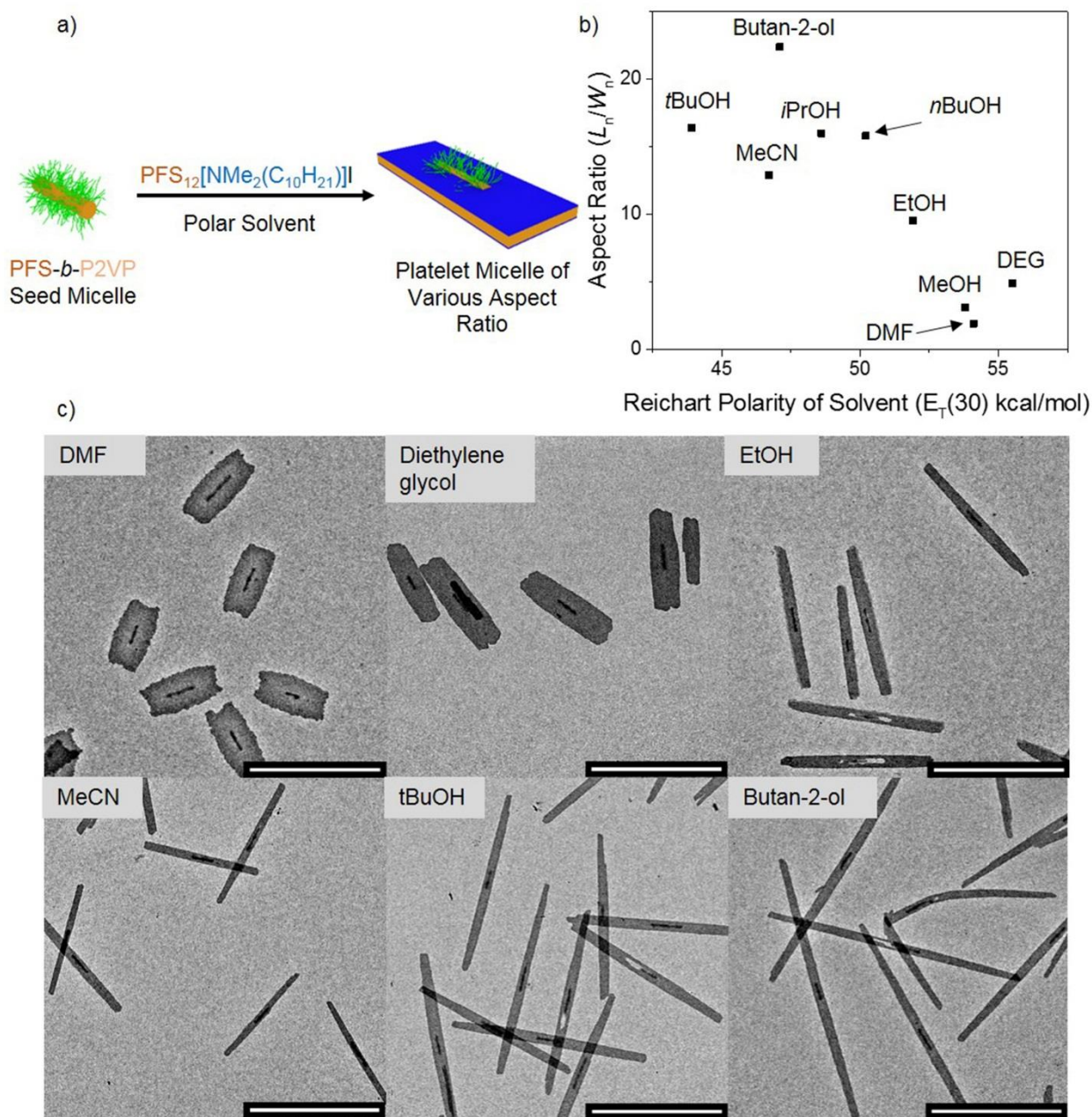


**Figure 5**. a) Cartoon schematic depicting the seeded growth of $PFS_{12}[NMe_2(C_{10}H_{22})]I$ from $PFS_{20}$-$b$-$P2VP_{180}$ seed micelles ($L_n$ = 260 nm, $L_w/L_n$ = 1.04) in solvents of varying polarity b) Graph displaying the observed platelet aspect ratio

($L_n/W_n$) vs the defined Reichart polarity of the solvent medium ($E_T(30)$ kcal/mol) c) Bright-field TEM images of 2D platelet micelles formed by seeded growth in various solvents. $m_{unimer}/m_{seed} = 10$ for every experiment. Scale bars = 2000 nm.

### d) Segmented 2D platelet co-micelle structures

Patchy platelet co-micelles were prepared from charge-terminated homopolymers by seeded growth of $PFS_{12}[NMe_3]I$ from previously prepared $PFS_{20}[PPh_2Me]I$ platelet micelles (Figure 6a). The phosphonium-capped $PFS_{20}[PPh_2Me]I$ platelet precursors were formed via seeded growth from 1D $PFS_{20}$-$b$-$P2VP_{180}$ micelles in $i$PrOH (Figure S14a-b) ($A_n = 1.0 \times 10^6$ nm$^2$, $A_w/A_n = 1.02$). Subsequent seeded growth of $PFS_{12}[NMe_3]I$ from the $PFS_{20}[PPh_2Me]I$ platelet micelles in $i$PrOH with $m_{unimer}/m_{seed} = 1$ yielded platelet co-micelle structures (Figure 6b-c). Interestingly, it was observed that $PFS_{12}[NMe_3]I$ crystallized preferentially in the terminal direction relative to the seed platelet, leaving the platelet width virtually unchanged. To quantify this, the average aspect ratio of both the platelet seeds and platelet co-micelles was calculated. The initial $PFS_{20}[PPh_2Me]I$ seed platelets had an aspect ratio ($L_n/W_n$) of 3.9 and this increased to 4.9 following the addition of $PFS_{12}[NMe_3]I$ at $m_{unimer}/m_{seed} = 1$. The preferential growth of $PFS_{12}[NMe_3]I$ on the $PFS_{20}[PPh_2Me]I$ platelet termini continued at higher $m_{unimer}/m_{seed}$ ratios to give platelet co-micelles of aspect ratios ($L_n/W_n$) up to 8.8 at $m_{unimer}/m_{seed} = 5$ (Figure S15, Supplementary Table 3). The platelet co-micelles were found to be colloidally unstable at $m_{unimer}/m_{seed} > 5$ and aggregation took place in solution as the lengths reached ca. 5 µm. It is noteworthy that in previous work cylinder-forming PFS-containing BCPs seeded by 2D platelet micelles with a crystalline PFS core have also shown a preference for epitaxial growth from the platelet termini to form hierarchical "scarf" structures.[50,62]

AFM analysis showed that the thickness of the platelet was consistent at ca. 8 nm across each segment of the platelet co-micelle, which again is presumably due to chain folding of the $PFS_{20}[PPh_2Me]I$ platelet (Figure S16), with a slight increase of *ca.* 1 nm in height at the interface between the two platelet segments. The theoretical length of a fully-chain-extended $PFS_{12}$ and $PFS_{20}$ in the absence of chain-folding is 8.5 nm and 13.8 nm, respectively. This implies that chain-folding occurs within the central $PFS_{20}[PPh_2Me]I$ platelet seed micelle, whereas the chains in flanking $PFS_{12}[NMe_3]I$ segments are fully- extended. The $PFS_{12}[NMe_3]I$ segments are discernible at each end by a slight increase in electron contrast, shown in the bright-field TEM images (Figure 6c). This could be due to chain-folding within the central $PFS_{20}[PPh_2Me]I$ platelet, which means there is a greater density of iodide counter-ions on the surface of the platelet on the terminal ammonium-functionalised areas.
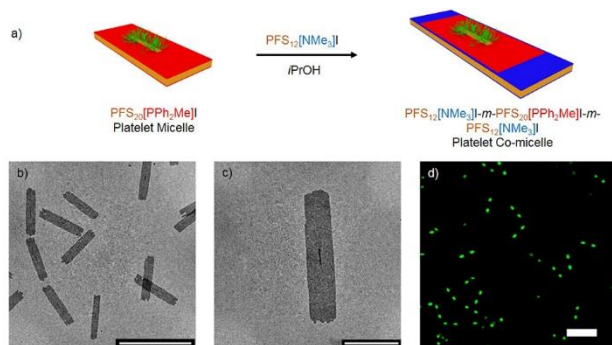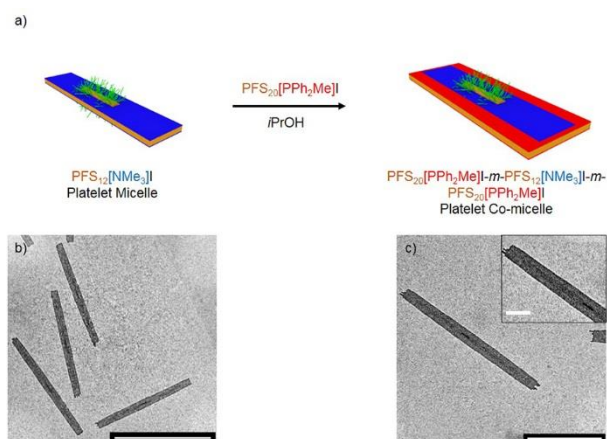
**Figure 6.** a) Cartoon schematic representation of the formation of platelet co-micelles through the growth of $PFS_{12}[NMe_3]I$ unimer solution in THF, seeded by $PFS_{20}[PPh_2Me]I$ platelets in *i*PrOH. b,c) A representative bright-field TEM image of the resultant platelet co-micelles and a higher magnification image of a single micelle. Platelet co-micelles were formed through the addition of $PFS_{12}[NMe_3]I$ unimer in THF to a solution of $PFS_{20}[PPh_2Me]I$ platelet micelles in *i*PrOH ($m_{unimer}/m_{seed}$ = 1). d) Laser scanning confocal microscopy image displaying platelet co-micelles formed through the seeded growth of one mass equivalent $PFS_{12}G/PFS_{12}[NMe_3]I$ 9:1 w/w blend of unimers from non-fluorescent $PFS_{20}[PPh_2Me]I$ platelet micelles in *i*PrOH. Scale bars = 4000 nm (b) 2000 nm (c) and 5000 nm (d).

The consistency in platelet height, irrespective of the increase in $DP_n$ of the core-forming block contrasts with previous observations of 1D cylindrical micelles, in which the height of the core were dependent upon the respective $DP_n$s of the crystalline core-forming block of the seeds and added unimer.[63] Previously reported heights of $PFS_{20}[PPh_2Me]I$ platelets by AFM were *ca.* 10 nm, which is consistent with the height of the micelles in this study.[50]

To demonstrate our method of producing 2D structures with spatially-confined surface chemistry, platelet co-micelles with fluorescent blocks at each end were formed by addition of a 1:9 blend by mass of $PFS_{12}[G]/PFS_{12}[NMe_3]I$ to $PFS_{20}[PPh_2Me]I$ platelet micelles in *i*PrOH (Figure 6d). The fluorescent segments are confined to each end of the platelet co-micelle, indicating that preferential seeded growth upon the platelet termini is consistent even when the charged-terminated unimer is blended with appreciable amounts of neutral homopolymer. Each segment of the $PFS_{12}[NMe_3]I$-*m*-$PFS_{20}[PPh_2Me]I$-*m*-$PFS_{12}[NMe_3]I$ 2D platelet co-micelle exhibited identical ED patterns by SAED analysis (Figure S17).[50] 3 pairs of identical ED spots were observed with a symmetry consistent with the monoclinic unit cell of a PFS single-crystal.[19] These results are also consistent with previous SAED analyses of PFS platelet co-micelles in the literature.[48,50]

As it was possible to increase the 2D platelet aspect ratio by seeded growth of $PFS_{12}[NMe_3]I$ from $PFS_{20}[PPh_2Me]I$ platelet micelles, seeded growth of $PFS_{20}[PPh_2Me]I$ from high-aspect-ratio $PFS_{12}[NMe_3]I$ platelets was attempted (Figure 7a). The $PFS_{12}[NMe_3]I$ high-aspect-ratio platelet precursors ($A_n$ = 7.97 x $10^3$ $nm^2$, $A_w/A_n$ = 1.04, $L_n/W_n$ = 16, Figure S14c-d) were prepared by the previously described seeded growth procedure (Figure 2a). Seeded growth of $PFS_{20}[PPh_2Me]I$ from the aforementioned $PFS_{12}[NMe_3]I$ platelets at $m_{unimer}/m_{seed}$ = 1 produced $PFS_{20}[PPh_2Me]I$-*m*-$PFS_{12}[NMe_3]I$-*m*-

13

PFS$_{20}$[PPh$_2$Me]I platelet co-micelles observed by bright-field TEM imaging (Figure 7b-c). The average aspect ratio of the PFS$_{12}$[NMe$_3$]I platelet seed structures from measurements of bright-field TEM images ($L_n/W_n$) was calculated to be 16. Following seeded growth of PFS$_{20}$[PPh$_2$Me]I at $m_{unimer}/m_{seed} = 1$ , the aspect ratio ($L_n/W_n$) of the platelet co-micelles was calculated to be 8.4, a reduction of approximately 50%. This is significant compared with the formation of PFS$_{12}$[NMe$_3$]I platelet micelles in $i$PrOH (discussed in Section b), as the aspect ratio decreased by only $ca.$ 20 % when the $m_{unimer}/m_{seed}$ value increased from 10 to 20 (Supplementary Table 2). Attempts to further explore the growth of platelet co-micelles at higher $m_{unimer}/m_{seed}$ values were unsuccessful due to observable defects at the interface between the PFS$_{12}$[NMe$_3$]I and PFS$_{20}$[PPh$_2$Me]I which in turn lead to cleavage and aggregation of the platelet co-micelles (Figure S18).



**Figure 7**. a) Cartoon schematic depicting the formation of platelet co-micelles through the seeded growth of PFS$_{20}$[PPh$_2$Me]I from high-aspect-ratio PFS$_{12}$[NMe$_3$]I platelets in $i$PrOH ($m_{unimer}/m_{seed} = 1$) . b,c) Representative bright-field TEM image of the formed structures with a higher magnification TEM image of a single micelle (inset scale bar = 500 nm). Scale bars = 4000 nm (b), 2000 nm (c).

SAED analysis of the platelet co-micelles showed that all three regions exhibited consistent ED patterns (Figure S19). Three identical pairs of ED spots corresponding to a monoclinic unit cell and characteristic d lattice spacing of 6.3 Å were observed, consistent with literature data for a PFS single-crystal.[19] A topological AFM image of a platelet co-micelle showed that the height changes slightly by $ca.$ 1 nm from $ca.$ 9 nm to $ca.$ 8 nm between the central and terminal segments (Figure S20), although the DP$_n$ for the core-forming block of the seed platelet micelle is 12 versus a value of 20 for the phosphonium-terminated outer segments. As the theoretical length of a fully-chain-extended PFS$_{12}$ and PFS$_{20}$ in the absence of chain-folding is 8.5 nm and 13.8 nm, respectively, this is again consistent with chain folding for the outer segments derived from PFS$_{20}$[PPh$_2$Me]I. A slight difference in height at the interface between the platelet co-micelle segments was observed ($ca$ 1.5 nm) which may be the result of a decrease in the areal density of the terminal groups due to chain folding in the peripheral PFS$_{20}$[PPh$_2$Me]I region (measured heights by AFM will include a small contribution from the end group and counter-anion).

14

### e) Influence of the counteranion on self-assembly

Previous studies have shown that seeded growth of $PFS_{20}[PPh_2Me]^+$ with $I^-$, $[BPh_4]^-$ and $C_6H_5CH_2SO_3^-$ counter-anions all yielded uniform, rectangular platelets in solution.[50] This suggests that the positively charged functional group is important and the counter-ion pairs less significant in terms of the 2D morphology obtained by seeded growth. It was proposed in the present study that exchange of $I^-$ counter ions for larger anions may have a greater effect upon the solution self-assembly of $PFS_{12}[NMe_3]I$, due to the relatively high charge density of the trimethylammonium cation.

Initially $I^-$ counteranions associated with $PFS_{12}[NMe_3]I$ homopolymers were exchanged for $[BPh_4]^-$ counteranions by addition of 200 molar equivalents of $Na[BPh_4]$ in MeOH to polymer solution in THF (Figure 8a). The displaced iodide counter ions and excess $Na[BPh_4]$ were removed by thorough extraction with methanol. Integration of observed phenyl proton $^1H$ NMR resonances and *Cp* protons associated with the PFS repeat units in the product was used to confirm quantitative counteranion exchange (Figure S21). Contact ion pairing of the counterion to the charged terminus of the polymer was confirmed by 2D DOSY $^1H$ NMR spectroscopy (Figure S22), as the diffusion coefficients corresponding to $[BPh_4]^-$ and $PFS[NMe_3]^+$ were equivalent ($D = 9.9 \times 10^{-10}$ $m^2$ $s^{-1}$). Seeded growth of $PFS_{12}[NMe_3][BPh_4]$ from $PFS_{20}$-*b*-$P2VP_{180}$ seeds ($L_n = 260$ nm, $L_w/L_n = 1.04$) in *i*PrOH yielded lenticular structures (Figure 8b), rather than the $PFS_{12}[NMe_3]I$ ribbon-like platelets that were formed by seeded growth under equivalent conditions (Figure 2). Seeded growth of $PFS_{12}[NMe_3][BPh_4]$ in methanol formed regular platelets, observed by bright-field TEM microscopy (Figure 8c) in contrast to the rather irregular platelet structures formed by $PFS_{12}[NMe_3]I$ (Figure 4b). The differences in the observed 2D morphologies obtained through seeded growth following anion exchange could be attributed to the large hydrophobic $[BPh_4]^-$ anion which changes the relative volume fraction of the hydrophilic terminus versus the hydrophobic $PFS_{12}$. The difference in solubility of the $PFS[NMe_3]I$ versus the $PFS[NMe_3][BPh_4]$ ion pairs in the solvent may also have an important effect.
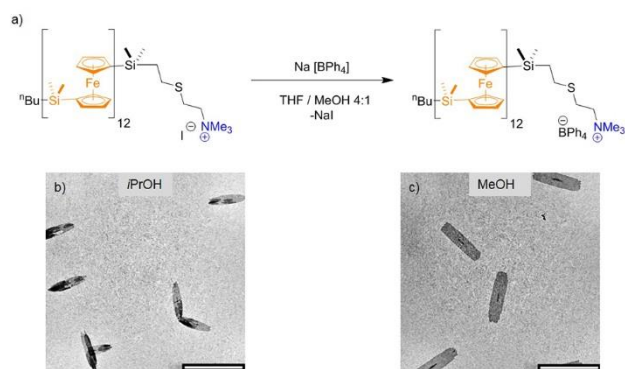


**Figure 8.** a) Scheme depicting the anion exchange process between $I^-$ and $[BPh_4]^-$ counteranions. b) Bright-field TEM image of lenticular platelets formed through seeded growth of $PFS_{12}[NMe_3][BPh_4]$ from $PFS_{20}$-*b*-$P2VP_{180}$ seed micelles ($L_n = 260$ nm, $L_w/L_n = 1.04$) in iPrOH. c) Bright-field TEM image of rectangular platelets formed through seeded growth of $PFS_{12}[NMe_3][BPh_4]$ from $PFS_{20}$-*b*-$P2VP_{180}$ seed micelles ($L_n = 260$ nm, $L_w/L_n = 1.04$) in MeOH. Scale bars = 2000 nm.

Anion exchange of [BPh$_4$]$^-$ for I$^-$ counter-ions attached to the PFS$_{23}$[NMe$_3$]$^+$ was shown to have a profound effect upon the colloidal stability of 2D platelets formed by seeded growth in solution. Seeded growth of PFS$_{23}$[NMe$_3$]I from PFS$_{20}$-$b$-P2VP$_{180}$ cylindrical seeds in $i$PrOH yielded aggregates of 2D platelets, observed by bright-field TEM microscopy (Figure 9a). After solutions of the platelet micelles were left for 12 h, a precipitate could be observed in the vial. It is apparent that the ammonium/iodide ion pair is unable to prevent rapid aggregation of the 2D platelet micelles following the seeded growth of PFS$_{23}$[NMe$_3$]I unimers. Association of [BPh$_4$]$^-$ anions led to uniform colloidally stable platelets being obtained by seeded growth of PFS$_{23}$[NMe$_3$][BPh$_4$] from PFS$_{20}$-$b$-P2VP$_{180}$ 1D micelles ($L_n$ = 260 nm, $L_w/L_n$ = 1.04) in $i$PrOH (Figure 9b). The bulky [BPh$_4$]$^-$ anion appears to provide highly effective charge balancing and colloidal stabilization relative to the iodide counterpart. AFM topological imaging showed the platelet micelle heights to be constant at $ca.$ 8.5 nm (Figure 9c). This indicates that chain-folding occurs within the PFS core of the PFS$_{23}$[NMe$_3$][BPh$_4$] platelet (the extended chain length of PFS$_{23}$ = 16 nm), consistent with the case of PFS$_{20}$[PPh$_2$Me]I platelet co-micelle segments in this study (Figure 6).

A linear relationship was observed between the $m_{unimer}/m_{seed}$ values and the platelet area indicative of a living-growth process in 2D (Figure S23, Supplementary Table 4). At high $m_{unimer}/m_{seed}$ ratios *(values* ≥ 15), spherical aggregates were observed by TEM imaging and persisted over a period of weeks, limiting the size of platelet micelles that could be obtained (Figure S24).
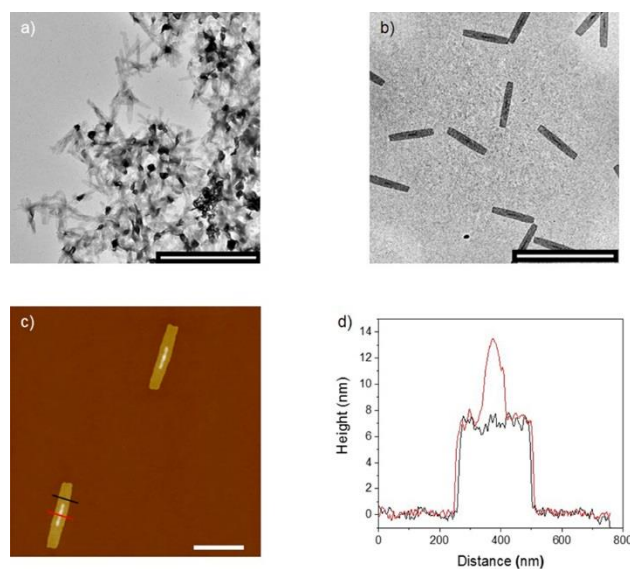


**Figure 9.** a) Bright-field TEM image of aggregates formed through attempted seeded growth of PFS$_{23}$[NMe$_3$]I by 1D PFS$_{20}$-$b$-P2VP$_{180}$ seed micelles in $i$PrOH before anion exchange. b) Representative bright-field TEM image of PFS$_{23}$[NMe$_3$][BPh$_4$] platelet micelles formed by seeded growth from PFS$_{20}$-$b$-P2VP$_{180}$ 1D micelles in $i$PrOH. c) Topological

AFM image of $PFS_{23}[NMe_3][BPh_4]$ micelles imaged on a carbon-coated TEM grid. d) Corresponding height trace of the regions marked in (c). $m_{unimer}/m_{seed}$ = 10. Scale bars = 4000 nm (a,b) and 1000 nm (c).

## Summary and Conclusions

Through the use of living anionic polymerization and post-polymerization modification with thiol-ene based "click" chemistry it was possible to synthesize a variety of $PFS_n$ homopolymers capped with hydrophilic ammonium termini. $PFS_{12}[NMe_3]I$ formed uniform, high-aspect-ratio 2D platelets in polar media through a seeded growth protocol. The high-aspect ratio platelet micelles were of controllable area, as demonstrated by the linear relationship between the $m_{unimer}/m_{seed}$ and $A_n$ values. The $PFS_{12}[NMe_3]I$ platelets consisted of fully chain-extended polymer chains without chain-folding based on AFM height analysis. The platelet micelles prepared to date were not colloidally stable in aqueous media and aggregated following dialysis from organic media into water. This is likely to be a result of the single ammonium charged functional group being unable to provide sufficient colloidal stability to the 2D platelet micelles with a highly hydrophobic crystalline PFS core. Potential methods to overcome this problem could be to introduce terminal groups bearing multiple charged centers, to use core-forming blocks of lower hydrophobicity, and/or to increase the hydrophilicity of the charged termini using groups such as $NH_3^+$. Studies of all of these approaches are currently in progress.

Variation in the length of the quaternizing alkyl chain led to insignificant differences in the solution self-assembly in *i*PrOH, yielding near-identical high-aspect-ratio platelet structures. The aspect ratio of 2D platelet micelles obtained by seeded growth in solution followed a general correlation with the polarity of the solvent medium, in which platelets formed by seeded growth in solvents of higher polarity exhibited lower aspect ratios.

The self-assembly behavior of the ammonium-terminated polyferrocene $PFS_{12}[NMe_3]I$ showed broad similarities but also key differences (for example in terms of resulting aspect ratios) when compared to the previously observed self-assembly behavior of charge-terminated $PFS_{20}[PPh_2Me]I$. Seeded growth of $PFS_{12}[NMe_3]I$ from $PFS_{20}[PPh_2Me]I$ platelet micelles occurred preferentially in the terminal direction of the $PFS_{20}[PPh_2Me]I$ platelet seeds, forming platelet co-micelles of increased aspect ratio. In contrast, seeded growth of $PFS_{20}[PPh_2Me]I$ unimers from high-aspect-ratio $PFS_{12}[NMe_3]I$ platelets resulted in a substantial decrease in platelet aspect ratio.

Exchange of $[BPh_4]^-$ for $I^-$ counter-ions of the hydrophilic ammonium termini was found to have a profound effect upon the 2D morphologies obtained in solution. Attempted seeded growth of $PFS_{23}[NMe_3]I$ in *i*PrOH resulted in platelets that rapidly precipitated from solution. In contrast, colloidally-stable $PFS_{23}[NMe_3][BPh_4]$ 2D platelet micelles were obtained under the same seeded growth conditions. Seeded growth of $PFS_{12}[NMe_3][BPh_4]$ in *i*PrOH yielded lenticular platelets whereas rectangular platelets were obtained in MeOH.

In this study we investigated the seeded growth of crystallizable homopolymers with hydrophilic ammonium moieties as stabilising terminal groups for the formation of 2D platelet micelles in polar solvents. New variables that affect the 2D platelet morphology and colloidal stability were determined, which include the polarity of the solvent medium in which seeded growth is conducted and the chemistry of the associated counteranion. To date there are currently relatively few examples of functional, colloidally stable 2D platelet nanostructures of high-aspect-ratio and examples based upon conjugated polymers are of great interest for nanoelectronic applications.[33,64,65] Application of the principles described in this study to other crystallizable charge-capped homopolymers should allow straightforward access to a variety of functional 2D assemblies in solution and studies along these lines are underway in our group. We are also performing detailed studies that aim to provide fundamental understanding of the factors that influence the observed aspect ratios for the 2D platelets formed by seeded growth.

## ASSOCIATED CONTENT

Supporting Information detailing experimental procedures, additional characterization data and related supplementary data are included. This material is available free of charge via the Internet at http://pubs.acs.org.

## AUTHOR INFORMATION

Corresponding Author

*To whom correspondence should be addressed: ian.manners@bris.ac.uk and imanners@uvic.ca

## ACKNOWLEDGMENT

## REFERENCES

(1)     Tritschler, U.; Pearce, S.; Gwyther, J.; Whittell, G. R.; Manners, I. *50th Anniversary Perspective* : Functional Nanoparticles from the Solution Self-Assembly of Block Copolymers. *Macromolecules* **2017**, *50* (9), 3439–3463.

(2)     Mai, Y.; Eisenberg, A. Self-Assembly of Block Copolymers. *Chem. Soc. Rev.* **2012**, *41* (18), 5969–5985.

(3)     Pochan, D. J.; Chen, Z.; Cui, H.; Hales, K.; Qi, K.; Wooley, K. L. Toroidal Triblock Copolymer Assemblies. *Science* **2004**, *306*, 94–97.

(4)     Jang, S. G.; Audus, D. J.; Klinger, D.; Krogstad, D. V; Kim, B. J.; Cameron, A.; Kim, S.-W.; Delaney, K. T.; Hur, S.-M.; Killops, K. L.; et al. Striped, Ellipsoidal Particles by Controlled Assembly of Diblock Copolymers. *J. Am. Chem. Soc.* **2013**, *135* (17), 6649–6657.

(5)     Gröschel, A. H.; Walther, A.; Löbling, T. I.; Schacher, F. H.; Schmalz, H.; Müller, A. H. E. Guided Hierarchical Co-Assembly of Soft Patchy Nanoparticles. *Nature* **2013**, *503* (7475), 247–251.

(6)     Dupont, J.; Liu, G. ABC Triblock Copolymer Hamburger-like Micelles, Segmented Cylinders, and Janus Particles. *Soft Matter* **2010**, *6* (15), 3654–3661.

(7)     Hayward, R. C.; Pochan, D. J. Tailored Assemblies of Block Copolymers in Solution: It Is All about the Process. *Macromolecules* **2010**, *43* (8), 3577–3584.

(8)     Keller, A. Polymer Single Crystals. *Polymer* **1962**, *3*, 393–421.

(9)     Holdsworth, P. J.; Keller, A. The Crystallization of Ethyl and Methyl Branched Copolymers of Polyethylene from Dilute Solution. *J. Polym. Sci. Part B Polym. Lett.* **1967**, *5* (8), 605–612.

(10)    Boott, C. E.; Nazemi, A.; Manners, I. Synthetic Covalent and Non-Covalent 2D Materials. *Angew. Chem. Int. Ed. Engl.* **2015**, *54*, 13876–13894.

(11)    Wang, J.; Lu, Y.; Chen, Y. Fabrication of 2D Surface-Functional Polymer Platelets via Crystallization-Driven Self-Assembly of Poly(ε-Caprolactone)-Contained Block Copolymers. *Polymer* **2019**, *160*, 196–203.

(12)    Dong, B.; Zhou, T.; Zhang, H.; Li, C. Y. Directed Self-Assembly of Nanoparticles for Nanomotors. *ACS Nano* **2013**, *7* (6), 5192–5198.

(13)    Li, B.; Li, C. Y. Immobilizing Au Nanoparticles with Polymer Single Crystals, Patterning and Asymmetric Functionalization. *J. Am. Chem. Soc.* **2007**, *129* (1), 12–13.

(14)    Mei, S.; Li, C. Y. Terraced and Smooth Gradient Polymer Brushes via a Polymer Single-Crystal Assisted Grafting-To Method. *Angew. Chemie* **2018**, *130* (48), 15984–15987.

(15)    Hailes, R. L. N.; Oliver, A. M.; Gwyther, J.; Whittell, G. R.; Manners, I. Polyferrocenylsilanes: Synthesis, Properties, and Applications. *Chem. Soc. Rev.* **2016**, *45*, 5358–5409.

(16)    Massey, J. A.; Temple, K.; Cao, L.; Rharbi, Y.; Raez, J.; Winnik, M. A.; Manners, I. Self-Assembly of Organometallic Block Copolymers: The Role of Crystallinity of the Core-Forming Polyferrocene Block in the Micellar Morphologies Formed by Poly(Ferrocenylsilane-b-Dimethylsiloxane) in n-Alkane Solvents. *J. Am.*

*Chem. Soc.* **2000**, *122* (47), 11577–11584.

(17)    Cao, L.; Manners, I.; Winnik, M. A. Influence of the Interplay of Crystallization and Chain Stretching on Micellar Morphologies: Solution Self-Assembly of Coil-Crystalline Poly (Isoprene-Block-Ferrocenylsilane). *Macromolecules* **2002**, *35*, 8258–8260.

(18)    Cambridge, G.; Gonzalez-Alvarez, M. J.; Guerin, G.; Manners, I.; Winnik, M. A. Solution Self-Assembly of Blends of Crystalline-Coil Polyferrocenylsilane-Block-Polyisoprene with Crystallizable Polyferrocenylsilane Homopolymer. *Macromolecules* **2015**, *48* (3), 707–716.

(19)    Hsiao, M.-S.; Yusoff, S. F. M.; Winnik, M. A.; Manners, I. Crystallization-Driven Self-Assembly of Block Copolymers with a Short Crystallizable Core-Forming Segment: Controlling Micelle Morphology through the Influence of Molar Mass and Solvent Selectivity. *Macromolecules* **2014**, *47* (7), 2361–2372.

(20)    Rizis, G.; van de Ven, T. G. M.; Eisenberg, A. Homopolymers as Structure-Driving Agents in Semicrystalline Block Copolymer Micelles. *ACS Nano* **2015**, *9* (4), 3627–3640.

(21)    Rizis, G.; van de Ven, T. G. M.; Eisenberg, A. "Raft" Formation by Two-Dimensional Self-Assembly of Block Copolymer Rod Micelles in Aqueous Solution. *Angew. Chem. Int. Ed. Engl.* **2014**, *53* (34), 9000–9003..

(22)    Yin, L.; Hillmyer, M. A. Disklike Micelles in Water from Polyethylene-Containing Diblock Copolymers. *Macromolecules* **2011**, *44* (8), 3021–3028.

(23)    Zheng, J. X.; Xiong, H.; Chen, W. Y.; Lee, K.; Van Horn, R. M.; Quirk, R. P.; Lotz, B.; Thomas, E. L.; Shi, A. C.; Cheng, S. Z. D. Onsets of Tethered Chain Overcrowding and Highly Stretched Brush Regime via Crystalline - Amorphous Diblock Copolymers. *Macromolecules* **2006**, *39* (2), 641–650.

(24)    Ganda, S.; Dulle, M.; Drechsler, M.; Förster, B.; Förster, S.; Stenzel, M. H. Two-Dimensional Self-Assembled Structures of Highly Ordered Bioactive Crystalline-Based Block Copolymers. *Macromolecules* **2017**, *50* (21), 8544–8553.

(25)    Xu, F.; Zhang, P.; Zhang, J.; Yu, C.; Yan, D.; Mai, Y. Crystallization-Driven Two-Dimensional Self-Assembly of Amphiphilic PCL- *b* -PEO Coated Gold Nanoparticles in Aqueous Solution. *ACS Macro Lett.* **2018**, *7* (9), 1062–1067.

(26)    Zhong, Y.; Wang, Z.; Zhang, R.; Bai, F.; Wu, H.; Haddad, R.; Fan, H. Interfacial Self-Assembly Driven Formation of Hierarchically Structured Nanocrystals with Photocatalytic Activity. *ACS Nano* **2014**, *8* (1), 827–833.

(27)    Su, M.; Huang, H.; Ma, X.; Wang, Q.; Su, Z. Poly(2-Vinylpyridine)-Block -Poly(ϵ-Caprolactone) Single

Crystals in Micellar Solution. *Macromol. Rapid Commun.* **2013**, *34* (13), 1067–1071.

(28)    Wang, J.; Zhu, W.; Peng, B.; Chen, Y. A Facile Way to Prepare Crystalline Platelets of Block Copolymers by Crystallization-Driven Self-Assembly. *Polymer* **2013**, *54* (25), 6760–6767.

(29)    Zhu, W.; Peng, B.; Wang, J.; Zhang, K.; Liu, L.; Chen, Y. Bamboo Leaf-Like Micro-Nano Sheets Self-Assembled by Block Copolymers as Wafers for Cells. *Macromol. Biosci.* **2014**, *14* (12), 1764–1770.

(30)    Inam, M.; Cambridge, G.; Pitto-Barry, A.; Laker, Z. P. L.; Wilson, N. R.; Mathers, R. T.; Dove, A. P.; O'Reilly, R. K. 1D vs. 2D Shape Selectivity in the Crystallization-Driven Self-Assembly of Polylactide Block Copolymers. *Chem. Sci.* **2017**, No. 8, 4223-4230.

(31)    Chen, W. Y.; Li, C. Y.; Zheng, J. X.; Huang, P.; Zhu, L.; Ge, Q.; Quirk, R. P.; Lotz, B.; Deng, L.; Wu, C.; et al. "Chemically Shielded" Poly(Ethylene Oxide) Single Crystal Growth and Construction of Channel-Wire Arrays with Chemical and Geometric Recognitions on a Submicrometer Scale. *Macromolecules* **2004**, *37* (14), 5292–5299.

(32)    Yang, S.; Shin, S.; Choi, I.; Lee, J.; Choi, T.-L. Direct Formation of Large-Area 2D Nanosheets from Fluorescent Semiconducting Homopolymer with Orthorhombic Crystalline Orientation. *J. Am. Chem. Soc.* **2017**, *139* (8), 3082–3088.

(33)    Han, L.; Wang, M.; Jia, X.; Chen, W.; Qian, H.; He, F. Uniform Two-Dimensional Square Assemblies from Conjugated Block Copolymers Driven by π –π Interactions with Controllable Sizes. *Nat. Commun.* **2018**, *9* (1), 865.

(34)    Wang, X.; Guerin, G.; Wang, H.; Wang, Y.; Manners, I.; Winnik, M. A. Cylindrical Block Copolymer Micelles and Co-Micelles of Controlled Length and Architecture. *Science* **2007**, *317* (5838), 644–647.

(35)    Gilroy, J. B.; Gädt, T.; Whittell, G. R.; Chabanne, L.; Mitchels, J. M.; Richardson, R. M.; Winnik, M. A.; Manners, I. Monodisperse Cylindrical Micelles by Crystallization-Driven Living Self-Assembly. *Nat Chem* **2010**, *2* (7), 566–570.

(36)    Boott, C. E.; Leitao, E. M.; Hayward, D. W.; Laine, R. F.; Mahou, P.; Guerin, G.; Winnik, M. A.; Richardson, R. M.; Kaminski, C. F.; Whittell, G. R.; et al. Probing the Growth Kinetics for the Formation of Uniform 1D Block Copolymer Nanoparticles by Living Crystallization-Driven Self-Assembly. *ACS Nano* **2018**, *12* (9), 8920–8933.

(37)    Petzetakis, N.; Dove, A. P.; O'Reilly, R. K. Cylindrical Micelles from the Living Crystallization-Driven Self-Assembly of Poly(Lactide)-Containing Block Copolymers. *Chem. Sci.* **2011**, *2* (5), 955–960.

(38)    Schmelz, J.; Schedl, A. E.; Steinlein, C.; Manners, I.; Schmalz, H. Length Control and Block-Type Architectures in Worm-like Micelles with Polyethylene Cores. *J. Am. Chem. Soc.* **2012**, *134* (34), 14217–14225.

(39)    Arno, M. C.; Inam, M.; Coe, Z.; Cambridge, G.; Macdougall, L. J.; Keogh, R.; Dove, A. P.; O'Reilly, R. K. Precision Epitaxy for Aqueous 1D and 2D Poly(ε-Caprolactone) Assemblies. *J. Am. Chem. Soc.* **2017**, *139* (46), 16980–16985.

(40)    Patra, S. K.; Ahmed, R.; Whittell, G. R.; Lunn, D. J.; Dunphy, E. L.; Winnik, M. A.; Manners, I. Cylindrical Micelles of Controlled Length with a π-Conjugated Polythiophene Core via Crystallization-Driven Self-Assembly. *J. Am. Chem. Soc.* **2011**, *133*, 8842–8845.

(41)    Kynaston, E. L.; Nazemi, A.; MacFarlane, L. R.; Whittell, G. R.; Faul, C. F. J.; Manners, I. Uniform Polyselenophene Block Copolymer Fiberlike Micelles and Block Co-Micelles via Living Crystallization-Driven Self-Assembly. *Macromolecules* **2018**, *51* (3), 1002–1010.

(42)    Jin, X.-H.; Price, M. B.; Finnegan, J. R.; Boott, C. E.; Richter, J. M.; Rao, A.; Menke, S. M.; Friend, R. H.; Whittell, G. R.; Manners, I. Long-Range Exciton Transport in Conjugated Polymer Nanofibers Prepared by Seeded Growth. *Science* **2018**, *360* (6391), 897–900.

(43)    Finnegan, J. R.; He, X.; Street, S. T. G.; Garcia-Hernandez, J. D.; Hayward, D. W.; Harniman, R. L.; Richardson, R. M.; Whittell, G. R.; Manners, I. Extending the Scope of "Living" Crystallization-Driven Self-Assembly: Well-Defined 1D Micelles and Block Comicelles from Crystallizable Polycarbonate Block Copolymers. *J. Am. Chem. Soc.* **2018**, *140* (49), 17127–17140.

(44)    Shin, S.; Menk, F.; Kim, Y.; Lim, J.; Char, K.; Zentel, R.; Choi, T.-L. Living Light-Induced Crystallization-Driven Self-Assembly for Rapid Preparation of Semiconducting Nanofibers. *J. Am. Chem. Soc.* **2018**, *140* (19), 6088–6094.

(45)    Tao, D.; Feng, C.; Cui, Y.; Yang, X.; Manners, I.; Winnik, M. A.; Huang, X. Monodisperse Fiber-like Micelles of Controlled Length and Composition with an Oligo(p-Phenylenevinylene) Core via "Living" Crystallization-Driven Self-Assembly. *J. Am. Chem. Soc.* **2017**, *139* (21), 7136–7139.

(46)    Hudson, Z. M.; Boott, C. E.; Robinson, M. E.; Rupar, P. A.; Winnik, M. A.; Manners, I. Tailored Hierarchical Micelle Architectures Using Living Crystallization-Driven Self-Assembly in Two Dimensions. *Nat Chem* **2014**, *6* (10), 893–898.

(47)    Qiu, H.; Gao, Y.; Boott, C. E.; Gould, O.; Harniman, R. L.; Richardson, R. M.; Miles, M. J.; Manners, I. Uniform and Hollow Rectangular Platelet Micelles from Crystallizable Polymer Blends. *Science* **2016**, *352*

(6286), 697.

(48) Nazemi, A.; He, X.; MacFarlane, L. R.; Harniman, R. L.; Hsiao, M.-S.; Winnik, M. A.; Faul, C. F. J.; Manners, I. Uniform "Patchy" Platelets by Seeded Heteroepitaxial Growth of Crystallizable Polymer Blends in Two Dimensions. *J. Am. Chem. Soc.* **2017**, *139* (12), 4409–4417.

(49) Yu, B.; Jiang, X.; Yin, J. Size-Tunable Nanosheets by the Crystallization-Driven 2D Self-Assembly of Hyperbranched Poly(Ether Amine) (HPEA). *Macromolecules* **2014**, *47* (14), 4761–4768.

(50) He, X.; Hsiao, M. S.; Boott, C. E.; Harniman, R. L.; Nazemi, A.; Li, X.; Winnik, M. A.; Manners, I. Two-Dimensional Assemblies from Crystallizable Homopolymers with Charged Termini. *Nat. Mater.* **2017**, *16* (4), 481–488.

(51) He, X.; He, Y.; Hsiao, M. S.; Harniman, R. L.; Pearce, S.; Winnik, M. A.; Manners, I. Complex and Hierarchical 2D Assemblies via Crystallization-Driven Self-Assembly of Poly(l -Lactide) Homopolymers with Charged Termini. *J. Am. Chem. Soc.* **2017**, *139* (27), 9221–9228..

(52) Inam, M.; Foster, J. C.; Gao, J.; Hong, Y.; Du, J.; Dove, A. P.; O'Reilly, R. K. Size and Shape Affects the Antimicrobial Activity of Quaternized Nanoparticles. *J. Polym. Sci. Part A Polym. Chem.* **2018**, *57*, 255–259.

(53) Inam, M.; Jones, J. R.; Pérez-Madrigal, M. M.; Arno, M. C.; Dove, A. P.; O'Reilly, R. K. Controlling the Size of Two-Dimensional Polymer Platelets for Water-in-Water Emulsifiers. *ACS Cent. Sci.* **2018**, *4* (1), 63–70.

(54) Rulkens, R.; Lough, A. J.; Manners, I. Anionic Ring-Opening Oligomerization and Polymerization of Silicon-Bridged [1]Ferrocenophanes: Characterization of Short-Chain Models for Poly(Ferrocenylsilane) High Polymers. *J. Am. Chem. Soc.* **1994**, *116* (2), 797–798.

(55) Lunn, D. J.; Boott, C. E.; Bass, K. E.; Shuttleworth, T. A.; McCreanor, N. G.; Papadouli, S.; Manners, I. Controlled Thiol-Ene Functionalization of Polyferrocenylsilane-Block-Polyvinylsiloxane Copolymers. *Macromol. Chem. Phys.* **2013**, *214* (24), 2813–2820.

(56) Bütün, V.; Armes, S. P.; Billingham, N. C. Selective Quaternization of 2-(Dimethylamino)Ethyl Methacrylate Residues in Tertiary Amine Methacrylate Diblock Copolymers. *Macromolecules* **2001**, *34* (5), 1148–1159.

(57) Wang, H.; Winnik, M. A.; Manners, I. Synthesis and Self-Assembly of Poly(Ferrocenyldimethylsilane- b -2-Vinylpyridine) Diblock Copolymers. *Macromolecules* **2007**, *40* (10), 3784–3789.

(58) Shen, L.; Wang, H.; Guerin, G.; Wu, C.; Manners, I.; Winnik, M. A. A Micellar Sphere-to-Cylinder Transition of Poly(Ferrocenyldimethylsilane-b-2-Vinylpyridine) in a Selective Solvent Driven by Crystallization. *Macromolecules* **2008**, *41* (12), 4380–4389.

23

(59)     Rulkens, R.; Lough, A. J.; Manners, I.; Lovelace, S. R.; Grant, C.; Geiger, W. E. Linear Oligo(Ferrocenyldimethylsilanes) with between Two and Nine Ferrocene Units: Electrochemical and Structural Models for Poly(Ferrocenylsilane) High Polymers. *J. Am. Chem. Soc.* **1996**, *118* (50), 12683–12695.

(60)     Gilroy, J. B.; Rupar, P. A.; Whittell, G. R.; Chabanne, L.; Terrill, N. J.; Winnik, M. A.; Manners, I.; Richardson, R. M. Probing the Structure of the Crystalline Core of Field-Aligned, Monodisperse, Cylindrical Polyisoprene-Block-Polyferrocenylsilane Micelles in Solution Using Synchrotron Small- and Wide-Angle X-Ray Scattering. *J. Am. Chem. Soc.* **2011**, *133* (42), 17056–17062.

(61)     Reichardt, C. Empirical Parameters of Solvent Polarity as Linear Free-Energy Relationships. *Angew. Chemie Int. Ed. English* **1979**, *18* (2), 98–110.

(62)     Gädt, T.; Ieong, N. S.; Cambridge, G.; Winnik, M. A.; Manners, I. Complex and Hierarchical Micelle Architectures from Diblock Copolymers Using Living, Crystallization-Driven Polymerizations. *Nat. Mater.* **2009**, *8* (2), 144–150.

(63)     Qiu, H.; Gao, Y.; Du, V. A.; Harniman, R.; Winnik, M. A.; Manners, I. Branched Micelles by Living Crystallization-Driven Block Copolymer Self-Assembly under Kinetic Control. *J. Am. Chem. Soc.* **2015**, *137* (6), 2375–2385.

(64)     Samorí, P.; Francke, V.; Müllen, K.; Rabe, J. P. Self-Assembly of a Conjugated Polymer: From Molecular Rods to a Nanoribbon Architecture with Molecular Dimensions. *Chem. Eur. J.* **1999**, *5* (8), 2312–2317.

(65)     Welte, L.; Calzolari, A.; Di Felice, R.; Zamora, F.; Gomez-Herrero, J. Highly Conductive Self-Assembled Nanoribbons of Coordination Polymers. *Nat Nano* **2010**, *5* (2), 110–115.

**For Table of Contents Use Only**